

# Mode conversion based on dielectric metamaterial in silicon

David Ohana and Uriel Levy\*

Department of Applied Physics, The Benin School of Engineering and Computer Science, The Hebrew University of Jerusalem, Jerusalem, 91904, Israel

\*ulevy@mail.huji.ac.il

**Abstract:** We propose, design and analyze a novel mode converter in silicon waveguide based on a graded index co-directional grating coupler. The device has a periodic variation in its refractive index along the propagation direction and a graded index profile along the transverse direction. The graded index profile is realized by the implementation of nanoscale dielectric metamaterial consisting of silicon features that are etched into the waveguide based on the concept of effective medium. Design considerations are discussed and analyzed in details in the framework of the coupled mode theory (CMT) and the effective medium theory (EMT). Using 3D finite difference time domain (FDTD) simulations we show that the mode converter can couple between different symmetric and asymmetric modes which are propagating along a single bus multimode waveguide. Mode purity on the order of 96%, crosstalk with the input mode of better than  $-23\text{dB}$ , and transmission of more than 96% can be obtained, with device length as short as  $20\mu\text{m}$ , and over  $\sim 25\text{nm}$  spectral bandwidth around the design wavelength of  $1550\text{nm}$ .

©2014 Optical Society of America

**OCIS codes:** (050.2065) Effective medium theory; (050.6624) Subwavelength structures; (130.3120) Integrated optics devices; (160.3918) Metamaterials.

---

## References and links

1. A. Shacham, K. Bergman, and L. P. Carloni, "Photonic Networks-on-Chip for future generations of chip multiprocessors," *IEEE Trans. Comput.* **57**(9), 1246–1260 (2008).
2. J. Ahn, M. Fiorentino, R. G. Beausoleil, N. Binkert, A. Davis, D. Fattal, N. P. Jouppi, M. McLaren, C. M. Santori, R. S. Schreiber, S. M. Spillane, D. Vantrease, and Q. Xu, "Devices and architectures for photonic chip-scale integration," *Appl. Phys., A Mater. Sci. Process.* **95**(4), 989–997 (2009).
3. M. J. Paniccia, "A perfect marriage: optics and silicon," *Optik & Photonik* **6**(2), 34–38 (2011).
4. I. Gasulla and J. Capmany, "1 Tb/s x km Multimode fiber link combining WDM transmission and low-linewidth lasers," *Opt. Express* **16**(11), 8033–8038 (2008).
5. S. Bigo, Y. Frignac, G. Charlet, W. Idler, S. Borne, H. Gross, R. Dischler, W. Poehlmann, P. Tran, C. Simonneau, D. Bayart, G. Veith, A. Jourdan, and J.-P. Hamaide, "10.2Tbit/s (256x42.7Gbit/s PDM/WDM) transmission over 100km TeraLight? fiber with 1.28bit/s/Hz spectral efficiency," in *Optical Fiber Communication Conference and International Conference on Quantum Information*, 2001 OSA Technical Digest Series (Optical Society of America, 2001), p. PD25.
6. J. Sakaguchi, Y. Awaji, N. Wada, A. Kanno, T. Kawanishi, T. Hayashi, T. Taru, T. Kobayashi, and M. Watanabe, "Space Division Multiplexed transmission of 109-Tb/s data signals using homogeneous seven-core fiber," *J. Lightwave Technol.* **30**(4), 658–665 (2012).
7. S. Berdagué and P. Facq, "Mode division multiplexing in optical fibers," *Appl. Opt.* **21**(11), 1950–1955 (1982).
8. R. Ryf, S. Randel, A. H. Gnauck, C. Bolle, A. Sierra, S. Mumtaz, M. Esmaelpour, E. C. Burrows, R.-J. Essiambre, P. J. Winzer, D. W. Peckham, A. H. McCurdy, and R. Lingle, "Mode-Division Multiplexing over 96 km of few-mode fiber using coherent  $6 \times 6$  MIMO processing," *J. Lightwave Technol.* **30**(4), 521–531 (2012).
9. M. Salsi, C. Koebele, D. Sperti, P. Tran, H. Mardoyan, P. Brindel, S. Bigo, A. Boutin, F. Verluise, P. Sillard, M. Astruc, L. Provost, and G. Charlet, "Mode-Division Multiplexing of  $2 \times 100$  Gb/s channels using an LCOS-based spatial modulator," *J. Lightwave Technol.* **30**(4), 618–623 (2012).
10. M. Blau and D. M. Marom, "Optimization of spatial aperture-sampled mode multiplexer for a three-mode fiber," *IEEE Photon. Technol. Lett.* **24**(23), 2101–2104 (2012).
11. X. Yu, W. T. Lau, and S. Fan, "Anomalous modal structure in a waveguide with a photonic crystal core," *Opt. Lett.* **31**(6), 742–744 (2006).
12. B. Desiatov, I. Goykhman, and U. Levy, "Nanoscale mode selector in silicon waveguide for on chip nanofocusing applications," *Nano Lett.* **9**(10), 3381–3386 (2009).

13. D. Dai, Y. Tang, and J. E. Bowers, "Mode conversion in tapered submicron silicon ridge optical waveguides," *Opt. Express* **20**(12), 13425–13439 (2012).
14. D. Dai and J. E. Bowers, "Novel concept for ultracompact polarization splitter-rotator based on silicon nanowires," *Opt. Express* **19**(11), 10940–10949 (2011).
15. Y. Ding, J. Xu, F. Da Ros, B. Huang, H. Ou, and C. Peucheret, "On-chip two-mode division multiplexing using tapered directional coupler-based mode multiplexer and demultiplexer," *Opt. Express* **21**(8), 10376–10382 (2013).
16. D. Dai, J. Wang, and Y. Shi, "Silicon mode (de)multiplexer enabling high capacity photonic networks-on-chip with a single-wavelength-carrier light," *Opt. Lett.* **38**(9), 1422–1424 (2013).
17. L.-W. Luo, N. Ophir, C. P. Chen, L. H. Gabrielli, C. B. Poitras, K. Bergmen, and M. Lipson, "WDM-compatible mode-division multiplexing on a silicon chip," *Nat. Commun.* **5**, 3069 (2014).
18. Y.-D. Yang, Y. Li, Y.-Z. Huang, and A. W. Poon, "Silicon nitride three-mode division multiplexing and wavelength-division multiplexing using asymmetrical directional couplers and microring resonators," *Opt. Express* **22**(18), 22172–22183 (2014).
19. H. Qiu, H. Yu, T. Hu, G. Jiang, H. Shao, P. Yu, J. Yang, and X. Jiang, "Silicon mode multi/demultiplexer based on multimode grating-assisted couplers," *Opt. Express* **21**(15), 17904–17911 (2013).
20. J. Castro, D. F. Geraghty, S. Honkanen, C. M. Greiner, D. Iazikov, and T. W. Mossberg, "Demonstration of mode conversion using anti-symmetric waveguide Bragg gratings," *Opt. Express* **13**(11), 4180–4184 (2005).
21. S.-Y. Tseng, Y. Kim, C. J. K. Richardson, and J. Goldhar, "Implementation of discrete unitary transformations by multimode waveguide holograms," *Appl. Opt.* **45**(20), 4864–4872 (2006).
22. F.-C. H. M.-C. Wu, "Adiabatic mode conversion in multimode waveguides using chirped computer-generated planar holograms," *IEEE Photon. Technol. Lett.* **23**, 807–809 (2011).
23. S.-Y. Tseng and M.-C. Wu, "Adiabatic mode conversion in multimode waveguides using computer-generated planar holograms," *IEEE Photon. Technol. Lett.* **22**(16), 1211–1213 (2010).
24. Y. Huang, G. Xu, and S.-T. Ho, "An ultracompact optical mode order converter," *IEEE Photon. Technol. Lett.* **18**(21), 2281–2283 (2006).
25. B.-T. Lee and S.-Y. Shin, "Mode-order converter in a multimode waveguide," *Opt. Lett.* **28**(18), 1660–1662 (2003).
26. M. Turduev, B. B. Oner, I. H. Giden, and H. Kurt, "Mode transformation using graded photonic crystals with axial asymmetry," *J. Opt. Soc. Am. B* **30**(6), 1569–1579 (2013).
27. J. Leuthold, J. Eckner, E. Gamper, P.-A. Besse, and H. Melchior, "Multimode interference couplers for the conversion and combining of zero- and first-order modes," *J. Lightwave Technol.* **16**(7), 1228–1239 (1998).
28. A. Hosseini, J. Covey, and R. Chen, "Mode order converter using tapered multimode interference couplers," in *Integrated Photonics Research, Silicon and Nanophotonics and Photonics in Switching*, OSA Technical Digest (CD) (Optical Society of America, 2010), p. IWB2.
29. V. Liu, D. A. B. Miller, and S. Fan, "Ultra-compact photonic crystal waveguide spatial mode converter and its connection to the optical diode effect," *Opt. Express* **20**(27), 28388–28397 (2012).
30. L. H. Frandsen, Y. Elesin, L. F. Frellsen, M. Mitrovic, Y. Ding, O. Sigmund, and K. Yvind, "Topology optimized mode conversion in a photonic crystal waveguide fabricated in silicon-on-insulator material," *Opt. Express* **22**(7), 8525–8532 (2014).
31. J. Lu and J. Vučković, "Objective-first design of high-efficiency, small-footprint couplers between arbitrary nanophotonic waveguide modes," *Opt. Express* **20**(7), 7221–7236 (2012).
32. G. Chen and J. U. Kang, "Waveguide mode converter based on two-dimensional photonic crystals," *Opt. Lett.* **30**(13), 1656–1658 (2005).
33. S. M. Rytov, "Electromagnetic properties of a finely stratified medium," *Sov. Phys. JETP* **2**, 466–475 (1956).
34. U. Levy, M. Nezhad, H.-C. Kim, C.-H. Tsai, L. Pang, and Y. Fainman, "Implementation of a graded-index medium by use of subwavelength structures with graded fill factor," *J. Opt. Soc. Am. A* **22**(4), 724–733 (2005).
35. U. Levy, M. Abashin, K. Ikeda, A. Krishnamoorthy, J. Cunningham, and Y. Fainman, "Inhomogeneous dielectric metamaterials with space-variant polarizability," *Phys. Rev. Lett.* **98**(24), 243901 (2007).
36. M. Grajower, G. M. Lerman, I. Goykhman, B. Desiatov, A. Yanai, D. R. Smith, and U. Levy, "Subwavelength plasmonics for graded-index optics on a chip," *Opt. Lett.* **38**(18), 3492–3495 (2013).
37. C. Della Giovampaola and N. Engheta, "Digital metamaterials" <http://arxiv.org/abs/1403.6488v1> [cond-mat.mtrl-sci] (2014).
38. J. B. Pendry, A. Aubry, D. R. Smith, and S. A. Maier, "Transformation optics and subwavelength control of light," *Science* **337**(6094), 549–552 (2012).
39. A. Yariv and P. Yeh, *Optical Waves in Crystals: Propagation and Control of Laser Radiation* (Wiley-Interscience, 2002).
40. J.-M. Liu, *Photonic Devices* (Cambridge, 2005).
41. P. Cheben, D.-X. Xu, S. Janz, and A. Densmore, "Subwavelength waveguide grating for mode conversion and light coupling in integrated optics," *Opt. Express* **14**(11), 4695–4702 (2006).
42. J. H. Schmid, P. Cheben, S. Janz, J. Lapointe, E. Post, A. Ge, A. Densmore, B. Lamontagne, P. Waldron, and D.-X. Xu, "Subwavelength grating structures in silicon-on-insulator waveguides," *Adv. Opt. Technol.* **2008**, e685489 (2008).
43. Lumerical Solutions, Inc., <http://www.lumerical.com/tcad-products/mode/>
44. Lumerical Solutions, Inc., <http://www.lumerical.com/tcad-products/fdtd/>

## 1. Introduction

Photonic integrated circuits (PICs) employing nano-photonic devices hold a great potential in the field of optical communication in general, and in particular in data communication for moderate ranges (~one to tens of meters, e.g. rack to rack communication) and short ranges (~one to tens of centimeters, e.g. board to board and chip to chip communication). Nowadays the communication at these ranges is mainly based on copper wires and interconnects, supporting limited bandwidth only. In the quest for continuous performance improvements in computing systems [1], communication rates between computers and between computer's components on/off chip, continue to increase [2,3] with copper technology reaching its physical limits [3]. In that manner, PICs can provide a proper solution for the growing need of high data rates by utilizing advanced photonic multiplexing technologies such as wavelength-division multiplexing (WDM) [4], polarization-division multiplexing (PDM) [5], spatial-division multiplexing (SDM) [6], and mode-division multiplexing (MDM) [7-10] which have been developed in the field of optical fiber communication.

MDM method exploits the orthogonality of the different spatial eigenmodes of a waveguide in order to encode separate data over each channel and multiplex the information over a multimode waveguide. A key component needed to realize a mode (de)multiplexer is a mode converter which ideally can couple any given spatial mode to any other desired mode. In the last few years intensive efforts were invested towards the realization of mode converters, and mode selectors [11,12] for the purpose of implementing MDM functionality in PICs [13-32]. The different methods can be divided to:

- Phase matching techniques based on adiabatic tapers [13-15], asymmetrical directional couplers [16-18], contra-directional grating assisted couplers [19-20] and directional grating couplers [21-23].
- Beam shaping techniques based on Mach-Zehnder interferometers [24], Multichannel branching waveguides [25], and asymmetric graded index structures [26].
- Constructive interference of coherent scattering based on Multimode interference (MMI) couplers [27,28] and programmed defects in waveguides [29-32].

All these methods have their advantages and deficiencies. For example, some methods, e.g. tapers [13] and contra-directional grating assisted couplers [19], usually require relatively large devices, while others, such as Mach-Zehnder interferometers [20] enable conversion of the first two modes only. Other methods such as those based on constructive interference of programmed defects [30] usually require ultra-fine features which may be difficult to fabricate. In this context, using the concept of directional grating couplers suggested in [21] can be very attractive. The approach is based on the implementation of a periodic structure along the propagation direction and a graded profile of refractive index in the transverse direction [Fig. 1(a)]. The periodic perturbation incorporated over the waveguide enables to perform mode conversion along the same waveguide, in contradiction to methods such as asymmetrical directional couplers, contra-directional grating assisted couplers or MMI couplers, which require two waveguides for the conversion. In addition, it can be designed to couple any desired pair of modes. Furthermore, its length can be controlled by the amplitude of the index variation. Yet, the physical approach for achieving the desired index profile remains a great challenge, in particular with high index materials such as silicon.

Here we take advantage of the effective medium concept for the purpose of achieving a mode converter in a high index platform such as silicon waveguide. The proposed device is based on a graded index co-directional grating coupler, which has a periodic variation in its refractive index along the propagation direction and a graded index profile along the transverse direction [Figs. 1(a)-1(b)]. The graded index profile is realized by using the effective medium concept in which a subwavelength grating consisting of alternating layers of  $n_1$  and  $n_2$  refractive indices with variable duty cycle [Figs. 1(b)-1(c)] is etched into the silicon waveguide. The period  $\Lambda$  of these layers is constant but the structure itself is not periodic, inasmuch as the width of the layers varies in a non-periodic fashion over the waveguide's

transverse direction. The desired refractive index profile is related to the grating features by the effective medium theory (EMT) approximation [33] which has numerous applications in controlling artificially the refractive index of structures, e.g. metamaterials and transformation optics [34-38]. For example, focusing lenses of different engineered index profiles were demonstrated in GaAs slab waveguide [34], silicon slab waveguide [35], plasmonics [36], and other metallic and dielectric structures [37]. The periodic structure along the propagation direction enables phase matching to the output mode due to the additional momentum provided by the grating, while the graded index profile accounts for maximizing the coupling strength by increasing the field overlap. With only few microns of length, our devices offer high mode purity, and low crosstalk when converting between any desired pair of modes. The approach is supported by analytic modeling and validated using full 3D finite difference time domain calculations. Schematic representation of the index profile of the device, and conceptual 3D model of the actual structure are shown in Figs. 1(a)-1(b).

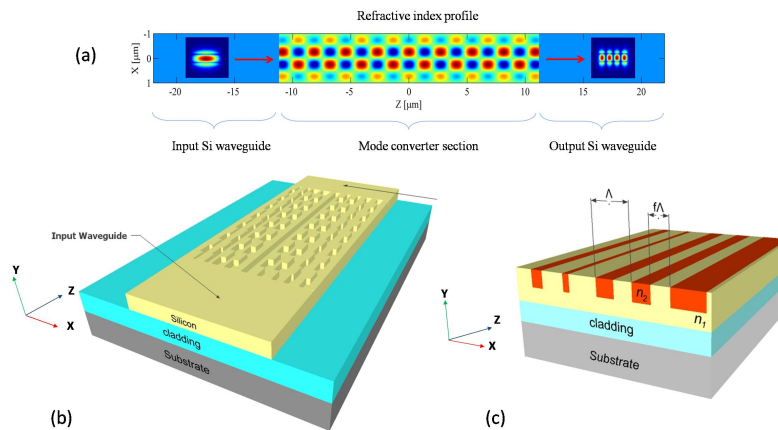


Fig. 1. (a) Schematic representation of the refractive index in the proposed device. Input and output waveguides have a constant refractive index of Si (3.46), while the converter section consists of a periodic variation in the propagation direction (z-axis) and has a graded index profile in the transverse direction (x-axis). The simulated modes are super imposed on the physical structure. (b) 3D conceptual model of the proposed mode converter. Si fraction relative to air varies across the x-axis and creates the required graded index profile along that direction. (c) Schematic representation of a waveguide with a graded index profile. Light propagates along the z axis while being confined in the core layer  $n_1$ . The duty cycle of the alternating layers  $n_1$  and  $n_2$  varies along the x axis in order to spatially control the effective index in that direction.

This paper is organized as follows: In Section 2 we describe the CMT and EMT which constitute the basic theories needed for the design and the analysis of the proposed device. In Section 3 we present some basic principles regarding our design method and the refractive index profile of the device. Design parameters and considerations for realizing the mode converter in addition to 3D FDTD simulation results and comprehensive comparison between different structures are presented in Section 4. Discussion and conclusions are provided in Section 5. More details regarding the CMT approach are provided in the Appendix.

## 2. Theory

### 2.1 Coupled mode theory (CMT)

Propagation of electromagnetic field in a perturbed dielectric structure can be approximated by the CMT [39,40]. In our case we assume the perturbation in the dielectric media,  $\Delta\epsilon(x,y,z)$ , to be periodic along the propagation direction z with a period  $\delta$ . According to the CMT the perturbation can result in energy coupling from one mode to another, and the amplitudes of each mode along the propagation are determined by a set of differential equations (see Appendix). If we designate  $\beta_m$  as the propagation constant in the z direction

corresponding to the  $m$ th guided mode, coupling occurs near the “phase matching” condition, i.e.  $(\beta_m - \beta_j - 2\pi q/\delta) = 0$  where  $q = 0, \pm 1, \pm 2, \dots$ . For this to happen the grating period should be chosen as to compensate for the  $\beta$  mismatch of the two modes. In addition, the coupling length (i.e. the position along the  $z$  axis in which 100% of the mode power couples to another mode) is inversely proportional to the coupling coefficient between the modes. The coupling coefficient is proportional to the spatial integration of the term  $E_m^*(x, y) \cdot \Delta \tilde{\epsilon}^{(q)}(x, y) \cdot E_j(x, y)$ , where  $E_m(x, y)$  and  $E_j(x, y)$  are the transverse cross sections of electric field of the  $m$ th and  $j$ th eigenmodes, and  $\Delta \tilde{\epsilon}^{(q)}(x, y)$  is the  $q$ 'th coefficient in the Fourier series of  $\Delta \epsilon(x, y, z)$  (see Appendix). We refer to this expression as the “field overlap” integral. Thus, proper choice of  $\Delta \epsilon(x, y, z)$  will maximize the coupling coefficient and minimize the coupling length.

To summarize this section, it turns out that in order to couple between modes “phase matching” should be satisfied by choosing the appropriate period of the perturbation along propagation direction. Once “phase matching” had been established, proper choice of the refractive index profile along the transverse direction is essential in order to achieve short coupling length.

## 2.2 Effective medium theory (EMT)

As will be explained later in the text, our goal is to construct a rectangular waveguide with a graded index profile in its transverse direction. This goal can be achieved by the effective medium concept [33]. By taking a periodic grating consisting of alternating layers of  $n_1$  and  $n_2$  refractive indices, with subwavelength period  $\Lambda$  and duty cycle  $f$  [Fig. 1(c)], the approximate solution for the effective index of the structure for TE (i.e.  $\mathbf{E} = E\hat{y}$ ) polarization is

$$n_{TE}^{(0)} = \sqrt{fn_1^2 + (1-f)n_2^2} \quad (1)$$

$$n_{TE}^{(2)} = \sqrt{\left[n_{TE}^{(0)}\right]^2 + \frac{1}{3} \left[ \frac{\Lambda}{\lambda} \pi f (1-f) (n_1^2 - n_2^2) \right]^2} \quad (2)$$

and for TM polarization (i.e.  $\mathbf{H} = H\hat{y}$ )

$$n_{TM}^{(0)} = \sqrt{\frac{n_1^2 \cdot n_2^2}{fn_2^2 + (1-f)n_1^2}} \quad (3)$$

$$n_{TM}^{(2)} = \sqrt{\left[n_{TM}^{(0)}\right]^2 + \frac{1}{3} \left[ \frac{\Lambda}{\lambda} \pi f (1-f) \left( \frac{1}{n_1^2} - \frac{1}{n_2^2} \right) \cdot \left[n_{TE}^{(0)}\right] \cdot \left[n_{TM}^{(0)}\right]^3 \right]^2} \quad (4)$$

where  $\lambda$  is the optical wavelength in vacuum and  $n_{TE}^{(0)}$ ,  $n_{TE}^{(2)}$  (and  $n_{TM}^{(0)}$ ,  $n_{TM}^{(2)}$ ) are the first two terms of the Taylor expansion of the effective index. The approximation is of reasonable accuracy when  $\Lambda \ll \lambda / \max(n_1, n_2)$ .

According to the above equations one can construct a subwavelength structure with a constant period and locally varying duty cycle in order to provide a spatial control over the effective index. We will use this method for generating a graded index profile in our mode converter. Recently, the effective medium concept has been used for the optimization of fiber to waveguide coupler [41,42].

## 3. Device principles

In this section the general principles for designing the index profile of the device are presented. In order to do so we first refer to the example of an 'ideal' device based on a continuous sinusoidal grating (i.e. a desired refractive index profile is assumed rather than

using the effective medium concept). Next, we discuss a more realistic case of a rectangular grating (again, without using the effective medium concept). After establishing the understanding of these devices and describing the general profile of the refractive index in both the longitudinal and the transverse dimensions we turn into discussing the practical implementation of an actual device in which the graded index profile along the transverse direction is realized by a subwavelength grating using the effective index concept. Comparison of the performances of all devices will be presented in section 4.

As mentioned before, the proposed device is a co-directional coupler which couples two eigenmodes propagating along the same direction in a single multimode waveguide. We assume an SOI platform, with  $2\mu\text{m}$  width and  $340\text{nm}$  height of Si waveguide ( $n_{\text{Si}} = 3.46$ ), having air as its upper cladding and  $\text{SiO}_2$  ( $n_{\text{SiO}_2} = 1.44$ ) as its bottom cladding (see Fig. 2). As an example, we aim at converting the TM0 to TM3 mode (which have dominant electric fields in  $\hat{y}$  direction).

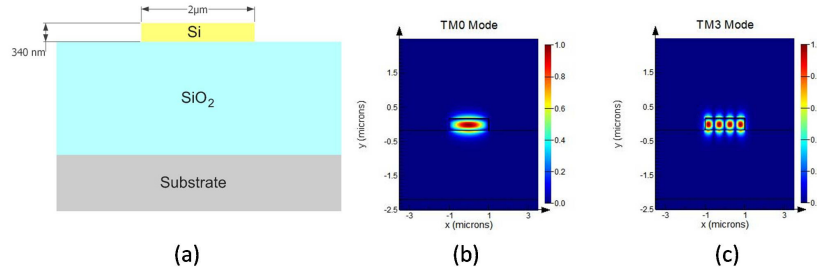


Fig. 2. (a) Waveguide cross section, (b-c) normalized  $E_{\hat{y}}$  field amplitude of the modes to be coupled.

We let the refractive index of the mode converter to vary in a sinusoidal fashion represented by

$$n(x, y, z) = n_0 + \Delta n(x, y, z) = n_0 + \Delta n(x, y) \cdot \exp[i(\beta_m - \beta_j)z] + c.c. \quad (5)$$

where  $n_0$  is the unperturbed part of the refractive index and  $\Delta n(x, y, z)$  represents the periodic perturbation along the propagation direction ( $z$  axis). Both are design parameters of our device. Expanding  $\Delta n(x, y, z)$  as a Fourier series we can define the  $q = 0, 1$  Fourier components of the sinusoidal grating, i.e.

$$\Delta \tilde{n}_{\text{sin}}^{(q=0)} = 0 \quad ; \quad \Delta \tilde{n}_{\text{sin}}^{(q=1)} = \Delta n(x, y) \quad (6)$$

Similarly to [21], here and in the following sections we calculate  $\Delta n(x, y)$  using the relation,

$$\Delta n(x, y) = \Delta n_{\text{max}} \cdot [E_y^{TM0}(x, y=0)]^* \cdot E_y^{TM3}(x, y=0) \quad (7)$$

where  $\Delta n_{\text{max}}$  is the maximal index modulation, and  $E_y^{TM0}(x, y=0)$  and  $E_y^{TM3}(x, y=0)$  are the unperturbed normalized electric field amplitude of the dominate component  $\hat{y}$ , at the middle of the waveguide (in the vertical direction i.e.  $y = 0$ ), for TM0 and TM3 modes, respectively. Since the  $\hat{y}$  components of the electric fields are identical in the vertical direction (the waveguide has a single vertical mode) for both TM0 and TM3 (see Fig. 2),  $\Delta n(x, y)$  is uniform along the  $y$  axis and index variation is only applied along along the horizontal  $x$  axis in order to control the overlap between the field of the two modes. This feature makes the fabrication of our proposed device much simpler. It should be noted that choosing  $\Delta n(x, y)$  as in Eq. (7) is not necessarily the best choice for maximizing the “field overlap” [Eq. (12)] and minimizing the coupling length, but according to the analytic calculations presented in the following design examples it is sufficient to achieve coupling length in the order of few microns.

To further simplify the implementation of our proposed device, we do not use materials other than silicon for the core waveguide. Thus, the maximal value of  $n(x,y,z)$  cannot exceed the refractive index  $n_{Si}$  and hence  $n_0$  should be smaller than  $n_{Si}$ . Note that one should perform calculation of Eq. (7) with respect to the modes of the unperturbed mode converter (i.e. a waveguide with refractive index of  $n_0$ ) rather than the original waveguide (i.e. a waveguide with refractive index of  $n_{Si}$ ). Otherwise, Eq. (5) shall contain an additional term  $n_{Si} - n_0$  which is considered as a constant perturbation. In that case  $\Delta\tilde{n}_{\sin}^{(q=0)} = n_{Si} - n_0$  which generates self-coupling of the mode, because  $\kappa_{00}^{(0)} \neq 0$  [Eq. (13)]. It is true however that this index mismatch will cause some loss due to Fresnel reflection. Yet, the small mismatch dictates a negligible reflection loss which is roughly estimated to be of  $\sim 0.15\%$  at each facet.

In order to quantify the device performances we first need to define some figures of merit. In all examples throughout this paper we have launched the TM<sub>0</sub> mode to the input waveguide and used 3D FDTD simulation to compute the electric field at the output. Decomposition of the computed field in the basis of the waveguide eigenmodes enables us to determine the power transmission of each mode through the device. We make use of these transmission results in order to compute three basic parameters: 1. Mode purity - defined as the ratio between output mode power (e.g. TM<sub>3</sub>) and the total transmitted power; 2. Crosstalk - defined as 10 times the 'log' of the ratio between the input mode power (i.e. TM<sub>0</sub>) and the output mode power (e.g. TM<sub>3</sub>); 3. Transmission - defined as the total transmitted power. Mode purity is of central importance as it reflects the ability of the device to couple the input mode to a specific desired mode rather than to other modes which can be part of the total transmitted power. In that manner, the crosstalk parameter is less important and was introduced in order to provide a comparison to other papers in the field. The transmission parameter is also important as it reflects the transmission efficiency of the device.

In Fig. 3 we present a numerical 3D FDTD calculation of light propagating through a mode converter based on a graded index sinusoidal grating, alongside a graph derived from the analytical calculation of the power exchange between the modes [Eqs. (15)-(16)]. The parameters used for this simulation are:  $n_0 = 3.2$ ,  $\Delta n_{\max} = 0.1$ , and  $\delta = 2\pi/\Delta\beta = 3.59\mu\text{m}$ . As expected, the FDTD simulation shows clear behavior of periodic power exchange, and the results are in good agreement with the analytic calculation. If we choose for example (see Fig. 4), the length of the mode converter to be  $6\mu\text{m}$  (i.e. at the first full power exchange location), we obtain high mode purity of 90%. Also, the crosstalk with the TM<sub>0</sub> is  $-15.4\text{dB}$ , and the total transmission is 98%. For a longer mode converter of  $18\mu\text{m}$  (i.e. at the second complete power exchange location), we obtain a mode purity of 89.2%, crosstalk with TM<sub>0</sub> of  $-17.5\text{dB}$ , and transmission of 98.5%.

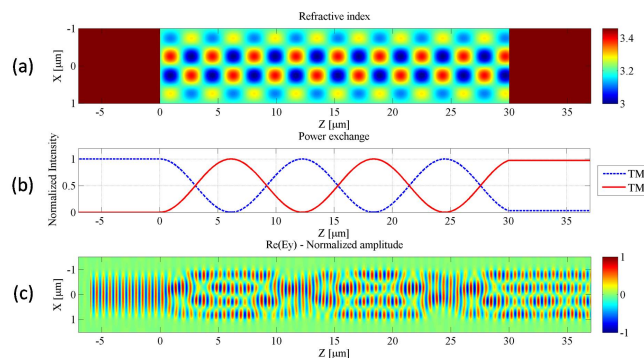


Fig. 3. TM<sub>0</sub> to TM<sub>3</sub> mode conversion with a graded index sinusoidal grating - (a) Refractive index profile of the device. The right and left uniform sections represent the input and output waveguides, and the intermediate segment between them is the converter section; (b) Analytic calculation of the power exchange between the two modes; (c) 3D FDTD simulation showing the Ey field (out of plane) propagation in the device.

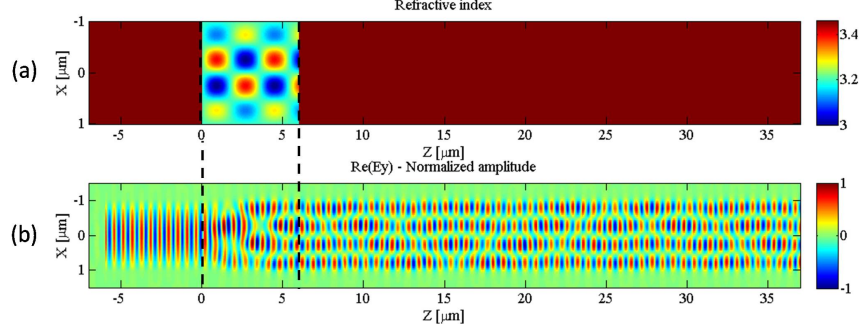


Fig. 4. TM0 to TM3 mode conversion with graded index sinusoidal grating - (a) Refractive index profile of the device. The right and left uniform sections represent the input and output waveguides, and the intermediate segment between them is the converter section; (b) 3D FDTD simulation showing the Ey field propagation in the device. Simulation parameters are the same as in Fig. 3 except for the converter length which is now restricted to 6μm (corresponding to the first complete power exchange location in Fig. 3). Dashed lines mark the converter section.

Realistically, changing the refractive index in a sinusoidal fashion over a very large index span is highly challenging. Thus, it is important to explore a simpler case of a rectangular grating. For such a case one obtains:

$$\Delta\tilde{n}_{rect}^{(q=0)} = (2 \cdot DC - 1) \cdot \Delta n(x, y) \quad ; \quad \Delta\tilde{n}_{rect}^{(q=1)} = 2\Delta n(x, y) \cdot DC \cdot \sin c(\pi \cdot DC) \quad (8)$$

where  $DC$  is the duty cycle of the grating. For a duty cycle of 50%  $\tilde{n}_{rect}^{(q=0)} = 0$  and  $\tilde{n}_{rect}^{(q=1)}$  is maximal and equals to  $0.63 \cdot \Delta\tilde{n}_{sin}^{(q=1)}$ . Similarly to the previous case, phase matching is still obtained, and thus one would still expect a complete power exchange to take place. Nevertheless, as the coupling coefficient is only 63% relative to the case of a sinusoidal grating, the conversion length, which is inversely proportional to the coupling coefficient, will increase by a factor of 1.58.

Another issue to be addressed in the case of a rectangular grating is whether there is coupling to radiating modes. In a sinusoidal grating coupling occurs only to a single mode, due to the fact that phase matching is satisfied at  $\beta_j \pm 2\pi/\delta$ . As we choose  $\delta$  such that  $\beta_j - 2\pi/\delta = \beta_m$  ( $\beta_m$  represents an eigenmode of the device),  $\beta_j + 2\pi/\delta = 2\beta_j - \beta_m$  which is most likely does not represent a waveguide mode (and even in the unlikely event that it is representing an eigenmode, the coupling coefficient to this mode is expected to be small because the graded index profile in x axis is not optimized for this mode). Also, in the case of coupling a lower mode to a higher mode (i.e.  $\beta_j > \beta_m$ ) one obtains  $2\beta_j - \beta_m > \beta_j$  and thus the term  $2\beta_j - \beta_m$  cannot represent a radiating mode which is above the “light line”. On the other hand, in rectangular grating phase matching is satisfied at  $\beta_j \pm q \cdot 2\pi/\delta = \beta_j(1 \pm q) \mp q \cdot \beta_m$ , and  $\beta_j(1-q) + q \cdot \beta_m$  can contain modes which are above the “light line”. Fortunately, the Fourier coefficients of a rectangular grating decay as a ‘sinc’ function and even more importantly the coupling coefficients are quickly vanishing due to poor overlap between the TM0 mode and the plane waves radiating modes. Therefore coupling to radiating modes is expected to be negligible. This conclusion is in good agreement with simulation results provided in the following section.

In Fig. 5 we present a 3D FDTD simulation of light propagation through a rectangular grating based mode converter with  $n_0 = 3.2$ ,  $\Delta n_{max} = 0.1$ ,  $DC = 50\%$ ,  $\delta = 3.59\mu\text{m}$  and  $9\mu\text{m}$  long mode converter. This length was chosen in order to coincide with the first complete power exchange. In that case, we obtain mode purity of 92%, crosstalk with TM0 of  $-17.5\text{dB}$  and transmission of 96.5%. As discussed in the previous section, some of the transmission losses may be caused by coupling to radiating modes. Additionally it can be caused by Fresnel reflections at the interface of the mode converter having  $n_0 = 3.2$  which is slightly



lower than the bulk Si materials used for the construction of the input and output waveguides. Although both loss mechanisms were not computed directly from the presented results, the high transmission relative to the sinusoidal grating (additional losses of only 1.5%) supports the claim that coupling to radiating modes is indeed small, especially when considering the additional loss mechanism of Fresnel reflections. Comparing the mode purity result to the case of a sinusoidal grating shows that it is  $\sim 2\%$  higher. We believe that further optimization of grating's period in the sinusoidal case, in order to fine tune the 'phase matching' condition will cancel this difference. Later on, when we perform a precise comparison between the different structures we will get back to this point. We also notice (not presented in the Figure) that there is still a periodic power exchange, as expected.

Next, we discuss the practical implementation of the proposed device. As mentioned before the obtained index profile should be achieved by the effective index medium and thus is discrete along the transverse direction. This is in contradiction to the previous examples, in which a continuous refractive index profile was assumed along the transverse axis. The discrete profile is approximated according to the EMT by varying the portion (i.e. the duty cycle) of Si and air in each period of the rectangular grating. Figure 6(a) shows the ideal continuous refractive index profile with rectangular grating (identical to Fig. 5(a)). Figure 6(b) shows the physical structure to be implemented in silicon. Figure 6(c) shows the obtained discrete refractive index profile according to the EMT.

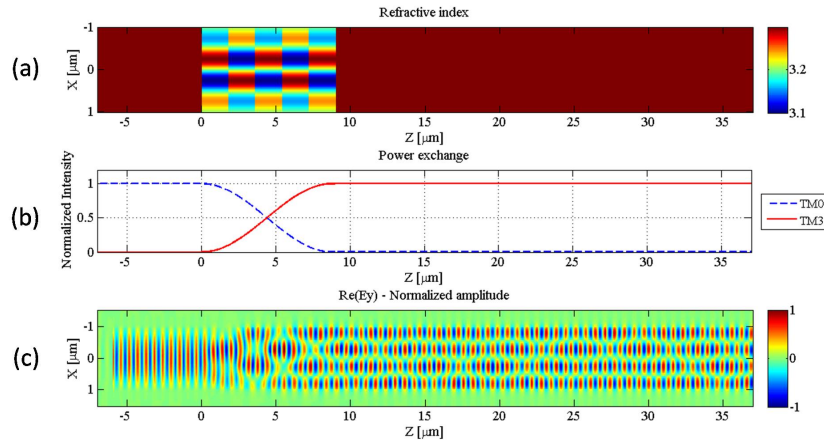


Fig. 5. TM0 to TM3 mode conversion with graded index rectangular grating - (a) Refractive index profile of the device. The right and left uniform sections are the input and output waveguides, and the intermediate segment between them is the converter section; (b) Analytic calculation of the power exchange between the two modes; (c) 3D FDTD simulation of the Ey field (out of plane) propagation in the device.

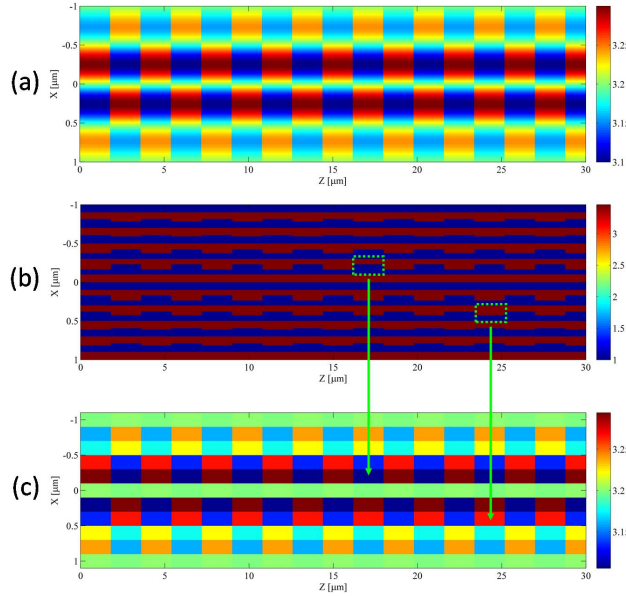


Fig. 6. Mapping between the EMT based graded index profile and the physical structure. (a) the desired refractive index profile (identical to Fig. 5(a)); (b) the physical binary grating structure; (c) the obtained discrete refractive index profile.

## 4. Numerical simulations

### 4.1 Design guidelines and considerations of a real device

After presenting the basic concept of the proposed device we can now turn to discuss the practical considerations and guidelines for determining the parameters of a real device in which the transverse refractive index profile is achieved by using a subwavelength grating following the effective medium concept. We devote this section to the design of an actual structure for the purpose of TM<sub>0</sub> to TM<sub>3</sub> mode conversion. It should be noted that while the polarization is TM from a waveguide perspective, it is TE from grating point of view. This observation becomes important when calculating the effective index according to Eqs.(1)-(4).

The basic structure, in which we incorporate the mode converter, is a standard SOI waveguide having cross sectional dimensions of 340nm height and 2μm width. We chose this width in order to obtain a reasonable difference in  $\beta$  between TM<sub>0</sub> and TM<sub>3</sub> modes. A wider waveguide results in a nearly undistinguishable wavevectors ( $\beta_m \approx \beta_j$ ) and it will be nearly impossible to couple energy from one mode to another.

First we need to determine the values of  $n_0$ ,  $\Delta n_{\max}$ ,  $n_1$  and  $n_2$ . As already mentioned,  $n_0$  and  $\Delta n_{\max}$  should be smaller than  $n_{Si}$  in order not to exceed Si refractive index. Still, there are additional considerations which one needs to take into account. On the one hand, higher values of  $n_0$  and  $\Delta n_{\max}$  will maximize the coupling coefficient, which is proportional to  $\Delta \tilde{\epsilon}^{(g)}(x, y) = 2\epsilon_0 n_0 \cdot \Delta \tilde{n}^{(g)}(x, y)$  ( $\epsilon_0$  is the vacuum permittivity). This is desired, as it provides a shorter coupling length and makes the device less sensitive to  $\beta$  mismatch (see Eqs. (15)-(16)). On the other hand the combination of  $n_0$ ,  $\Delta n_{\max}$ ,  $n_1$  and  $n_2$  affects the minimal feature size of Si and air, and one should choose their combination taking into account fabrication constraints. In our design, we restricted the minimal period to be  $\Lambda = 200\text{nm}$  and the minimal feature size (of either Si or air gap) to be 50nm. These are typical values that can be fabricated with modern technology. Moreover, lower values of  $n_0$  will increase Fresnel reflections and losses in the mode converter facets due to the index mismatch to  $n_{Si}$ . Taking the above mentioned considerations into account, we find the values of  $n_0 = 3.35$ ,  $\Delta n_{\max} = 0.055$ ,  $n_1 = 3.46$  and  $n_2 = 3.22$  to be reasonable. This set of parameters was chosen as it

provides the shortest coupling length ( $< 20\mu\text{m}$ ) among many sets of parameters that were considered. With these values we can implement 10 periods over the waveguide's width with  $\Lambda = 200\text{nm}$  and the minimum features size of air gap and Si are  $\sim 50\text{nm}$  and  $\sim 62\text{nm}$  respectively.

Next, we need to determine the grating's period along the propagation direction. A commercial-grade simulator eigenmode solver and propagator [43] was used to perform the calculations of the field profiles and the effective indices of the modes. As explained before, in order to avoid self coupling, all calculations were performed on a waveguide with  $n_0$  as the bulk core index. The effective indices of the modes at the target wavelength of  $1550\text{nm}$  are 2.591 and 2.186 for TM0 and TM3 respectively. Those values were used to calculate the grating period  $\delta = 2\pi / (\beta_{TM0} - \beta_{TM3}) = 3.84\mu\text{m}$ . As explained before, in order to maximize the first Fourier component of the dielectric perturbation we chose a grating duty cycle of 50%. Because  $n_0$  is an approximation of the 'dc' term of the refractive index of the structure using the EMT, further optimization of the grating period is needed in order to fine tune the 'phase matching' condition. After some iterative simulations, with 'mode purity' as the basic criterion for optimization, the exact period was determined to be  $3.64\mu\text{m}$ . The same optimization procedure will be performed also for the continuous sinusoidal and rectangular gratings presented later as a bench-mark comparison, as the effective 'dc' term of the refractive index for each structure is not exactly the same.

The last parameter to be defined is the required etching depth. As previously mentioned, our goal is to construct a device with effective index profile which is varying around an average value of  $n_0 = 3.35$  with a maximal variation of  $\Delta n_{\text{max}} = 0.055$ , using alternating layers which have bulk indices of  $n_1 = 3.46$  and  $n_2 = 3.22$ . While the refractive index of 3.46 is the bulk index of silicon, the other refractive index of 3.22 has to be artificially generated via etching, knowing that it is possible to obtain similar mode index for two waveguides with different core materials simply by controlling their geometry. Accordingly, we have calculated the TM0 mode index of a  $2\mu\text{m} \times 340\text{nm}$  waveguide with 3.22 core index and obtained  $n_{\text{eff}}^{\text{TM0}} = 2.444$ . The same mode index was achieved by considering a silicon waveguide (bulk index of 3.46) with a cross section of  $2\mu\text{m} \times 290\text{nm}$ . Thus, etching depth of  $50\text{nm}$  relative to the original height should be sufficient in order to achieve 3.22 effective bulk index.

Figure 7 shows 3D conceptual model of the device designed according to the above parameters. In Fig. 8(a) we present the actual refractive index profile of the device.

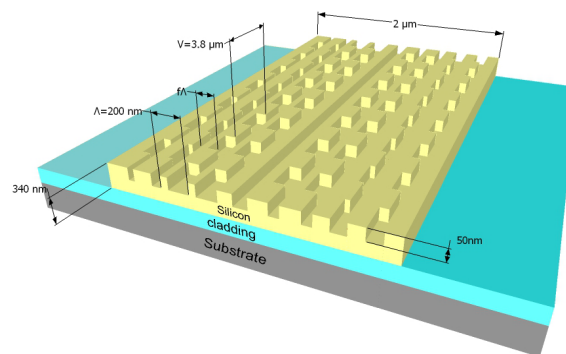


Fig. 7. 3D conceptual model of the proposed device.

#### 4.2 Results

A commercial-grade simulator based on the finite-difference time-domain method [44] was used to perform 3D beam propagation through the EMT based graded index rectangular grating mode converter. In Fig. 8(b) we present the  $E_y$  field profile along the device, together with the analytic calculation of the power exchange between the modes [Fig. 8(c)]. The length

of the mode converter is  $18.5\mu\text{m}$ . We obtained mode purity of 96.8%, crosstalk with TM0 of  $-23.9\text{dB}$ , and the total transmission of 96%. In the next section we will compare these results to those obtained with the continuous sinusoidal and rectangular structures.

We also tested the TM0 to TM3 mode converter spectral sensitivity around the design wavelength of  $1550\text{nm}$ . The results are plotted in Fig. 9 where it can be seen that the device maintains mode purity above 90% and crosstalk of less than  $-12.5\text{dB}$  for about  $25\text{nm}$  spectral range. We believe that the bandwidth can be further optimized by changing the design parameters of the device (e.g.  $n_0$ ,  $n_2$  and etching depth).

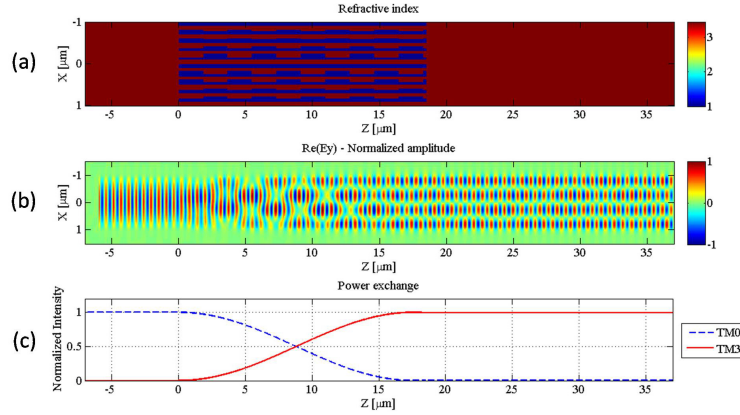


Fig. 8. TM0 to TM3 mode conversion with EMT based graded index rectangular grating - (a) Refractive index profile of the device. The right and left uniform sections represent the input and output waveguides, and the intermediate segment between them is the converter section; (b) 3D FDTD simulation of the Ey field (out of plane) propagation in the device; (c) Analytic calculation of the power exchange between the two modes.

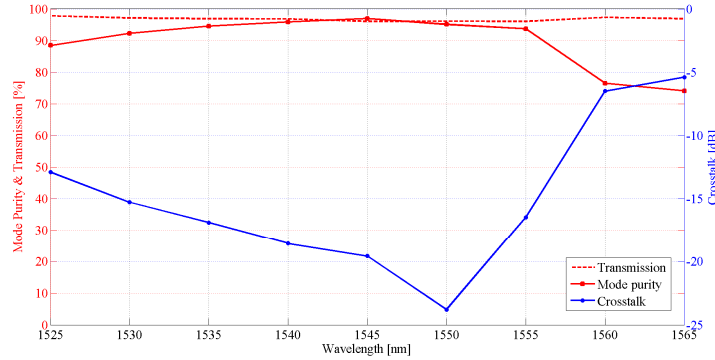


Fig. 9. Mode purity, transmission and crosstalk vs. wavelength for the TM0 to TM3 mode converter.

#### 4.3 Comparison to continuous sinusoidal and rectangular structures

In this section we compare the performance of our device presented in section 4.2 to the cases of ideal structures (i.e. not based on the effective index concept) varying in a sinusoidal or rectangular fashion. All the parameters are the same as for the aforementioned device, except for the grating's period which, as mentioned before, was optimized separately for each case to maximize the mode purity. In both cases we obtained highest mode purity with grating period of  $4.02\mu\text{m}$ . The comparison summary is presented in Table 1.

**Table 1. Comparison between the ‘ideal’ structures and the real device**

Parameter	'Ideal' Sinusoidal	'Ideal' Rectangular	Real Device
Mode Purity	96.1%	96.1%	96.8%
Transmission	98.3%	96.7%	96%
Crosstalk	-25.7dB	-23.3dB	-23.9dB
Coupling Length	11 $\mu$ m	18.5 $\mu$ m	18.5 $\mu$ m

As can be observed, the ideal sinusoidal structure shows better performances in its transmission and crosstalk, although the differences are minor. The ideal rectangular structure is similar to the real device in all three figures of merit. Comparing the performances of both the ideal rectangular structure and the real device to the ideal sinusoidal structure, it is again evident that losses caused by coupling to radiating modes and Fresnel reflections at the interface between the waveguides and the mode converter are very small, in the order of  $\sim 2\%$ . Coupling length for the rectangular structures is longer than achieved by the sinusoidal structure by a factor of 1.68 which is in fair agreement with the expected factor of 1.58.

#### 4.4 Mode conversion between symmetric and anti-symmetric modes

To demonstrate the capability of the effective medium approach to perform mode conversion to both symmetric and anti-symmetric modes we show two additional examples of mode converters designed for coupling TM<sub>0</sub> to TM<sub>2</sub> and TM<sub>0</sub> to TM<sub>1</sub> modes, following the design guidelines mentioned before. In Fig. 10 we present the calculated  $E_y$  field profile along the device. Efficient conversion of TM<sub>0</sub> to TM<sub>1</sub> for a 2 $\mu$ m wide waveguide is challenging, because their wavevectors are very close, preventing from coupling to occur, as explained before. Therefore, TM<sub>0</sub> to TM<sub>1</sub> mode conversion was demonstrated for a 1 $\mu$ m wide waveguide, where their wavevectors are distinguishable. For TM<sub>0</sub> to TM<sub>1</sub> coupling and device length of 20 $\mu$ m we obtained mode purity of 96.4%, crosstalk with TM<sub>0</sub> of -27.9dB, and total transmission of 97%. For TM<sub>0</sub> to TM<sub>2</sub> coupling and device length of 19 $\mu$ m we obtained mode purity of 93.9%, crosstalk with TM<sub>0</sub> of -45.1dB, and total transmission of 97%.

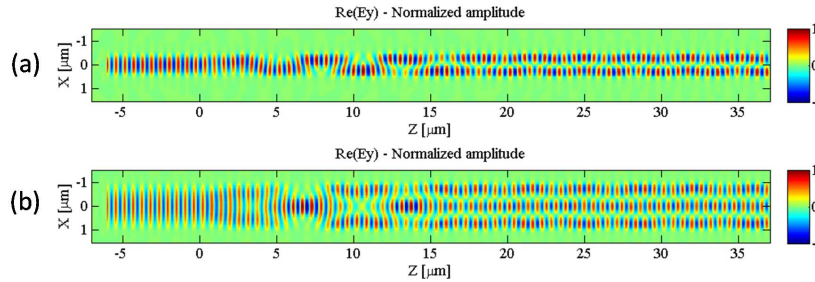


Fig. 10. TM<sub>0</sub> to TM<sub>1</sub> and TM<sub>2</sub> mode conversion with EMT based graded index rectangular grating - (a) 3D FDTD simulation of the  $E_y$  field (out of plane) propagation in a TM<sub>0</sub> to TM<sub>1</sub> mode converter. Simulation parameters are:  $n_0 = 3.35$ ,  $\Delta n_{\max} = 0.055$ ,  $\Lambda = 100\text{nm}$ , etching depth of 50nm,  $\delta = 5.3\mu\text{m}$ ,  $DC = 50\%$ , and converter length of 20 $\mu\text{m}$ . (b) 3D FDTD simulation showing the  $E_y$  field (out of plane) propagation in a TM<sub>0</sub> to TM<sub>2</sub> mode converter. Simulation parameters are:  $n_0 = 3.35$ ,  $\Delta n_{\max} = 0.055$ ,  $\Lambda = 200\text{nm}$ , etching depth of 50nm,  $\delta = 7\mu\text{m}$ ,  $DC = 50\%$ , and converter length of 19 $\mu\text{m}$ .

## 5. Discussion and summary

A mode converter based on graded index co-directional grating coupler in SOI is proposed, designed and analyzed. Design considerations are discussed in details. The proposed concept is attractive mainly for realizing mode division multiplexers and de-multiplexers. This can be achieved e.g. by fabricating few single mode waveguides on a single chip, converting the fundamental mode in each of these waveguides to a different higher mode and finally combine the outputs of these waveguides into a single multimode bus waveguide or fiber. The

proposed approach can also be useful for coupling between various waveguides (e.g. photonic crystal or slot waveguides). We showed that the mode converter can couple between different symmetric and asymmetric modes which are propagating in a single multimode waveguide. Mode purity of ~96%, crosstalk with the input mode better than -23dB, and transmission better than 96% can be obtained, with device length of ~20μm, over ~25nm spectral bandwidth around the design wavelength of 1550nm. Device length can be further reduced, e.g. by choosing a transverse index profile different than the one in Eq. (7), to maximize the coupling efficiency (i.e. field overlap). Alternatively, the device length can be reduced by using higher refractive index modulation, albeit at the expense of increased fabrication complexity.

Mode converters can be designed to perform optimal coupling between two specific desired modes, while barely affecting other modes. Accordingly, one can think of superimposing several such devices within the bus waveguide. As an example, with proper design such that several mode converters will all have the same coupling length (e.g. by wisely choosing transverse index profile or  $\Delta n_{\max}$ ), one may use this concept to implement a multi-mode to a single mode converter.

As a final comment, for all the examples provided in the paper we have assumed an SOI platform with silicon as a core, and air as an upper cladding. However, for many practical applications, silica upper cladding may be preferred e.g. as a passivation layer. It should be noted that our approach can easily support such geometry. While the same principles and guidelines mentioned in the text should still be valid, the optimized values of the parameters will obviously be different in order to account for the effect of replacing the upper air cladding with silica upper cladding.

## 6. Appendix - Coupled mode theory

The basic equations and principles of the CMT used in the paper were introduced in [39,40]. Here we only present briefly the final equations needed for understanding the concept of 'phase matching', 'coupling coefficient', 'field overlap' and the analytic calculation of the power exchange in a co-directional coupler.

In the proposed device we assume the perturbation to be periodic in the propagation direction  $z$ . The dielectric function of the structure is written as

$$\varepsilon(x,y,z) = \varepsilon_0(x,y,z) + \Delta\varepsilon(x,y,z) \quad (9)$$

where  $\varepsilon_0(x,y,z)$  is the unperturbed dielectric media and  $\Delta\varepsilon(x,y,z)$  represents the periodic perturbation of a period  $\delta$ . It is assumed that the perturbation is weak relative to  $\varepsilon_0(x,y,z)$ .

According to the CMT the perturbation results in energy coupling between one mode and another. The electric field propagated in a perturbed waveguide which supports  $M$  modes, is represented by a superposition of all the possible  $E_m(x,y)$  eigenmodes

$$E(x,y,z,t) = \sum_1^M A_m(z) E_m(x,y) e^{i(\omega t - \beta_m z)} \quad (10)$$

where  $m$  is the mode subscript,  $A_m(z)$  is the amplitude,  $\beta_m$  is the propagation constant in the  $z$  direction corresponding to the  $m$ th guided mode and  $\omega$  is the angular frequency.  $A_m$  is  $z$  depended so it reflects the energy coupling between guided modes due to the perturbation.

Given the fact that the dielectric perturbation is periodic in  $z$  we can expand it as a Fourier series and retrieve  $A_m(z)$ , which represents the amplitude evolution along the propagation axis, by the following set of differential equations

$$\frac{d}{dz} A_m = -i \sum_j \sum_q \kappa_{mj}^{(q)} A_j e^{i(\beta_m - \beta_j - \frac{q2\pi}{\delta})z} \quad (11)$$

$\kappa_{mj}^{(q)}$  is the coupling coefficient which reflects the coupling strength of the  $j$ th mode to the  $m$ th mode due to the  $q$ th Fourier coefficient of the perturbation's Fourier expansion. It is defined as

$$\kappa_{mj}^{(q)} = \frac{\omega}{4} \int_{-\infty}^{\infty} \int_{-\infty}^{\infty} E_m^*(x, y) \cdot \Delta\tilde{\varepsilon}^{(q)}(x, y) \cdot E_j(x, y) dx dy \quad (12)$$

where  $\Delta\tilde{\varepsilon}^{(q)}$  is the  $q$ th Fourier coefficient of  $\Delta\varepsilon(x, y, z)$ . The coupling length is inversely proportional to  $\kappa_{mj}^{(q)}$ .

As stated before, according to Eq. (11), assuming the amplitude  $A_m(z)$  is varying slowly in space, coupling will occur near the ‘‘phase matching’’ condition, i.e.  $(\beta_m - \beta_j - 2\pi q/\delta) = 0$ . For this to happen the grating period should be chosen as to compensate for the  $\beta$  mismatch of the two modes. In addition, according to Eq. (12), for a constant perturbation,  $\Delta\tilde{\varepsilon}^{(q)}$  will also be a constant and the coupling coefficient will vanish due to the orthogonality of the modes. Therefore,  $\Delta\tilde{\varepsilon}^{(q)}$  must vary along  $(x, y)$  in order to maximize the overlap integral in Eq. (12) by as much as needed so as to achieve a desired coupling length. An example for choosing  $\Delta\varepsilon(x, y, z)$  is presented in the main text where we assumed refractive index perturbation as in Eq. (7). Substituting  $\Delta\tilde{\varepsilon}^{(q)}(x, y) = 2\epsilon_0 n_0 \cdot \Delta\tilde{n}^{(q)}(x, y)$  into Eq. (12) we obtain:

$$\kappa_{mj}^{(q)} = \frac{\omega\epsilon_0 n_0}{2} \int_{-\infty}^{\infty} \int_{-\infty}^{\infty} E_m^*(x, y) \cdot \Delta\tilde{n}^{(q)}(x, y) \cdot E_j(x, y) dx dy \quad (13)$$

By combining this term, e.g. with  $\Delta\tilde{n}^{(q)}$  from Eq. (6)-(7) we get

$$\kappa_{mj}^{(q=1)} = \frac{\omega\epsilon_0 n_0}{2} \int_{-\infty}^{\infty} \int_{-\infty}^{\infty} \Delta n_{\max} \cdot |E_m(x, y)|^2 \cdot |E_j(x, y)|^2 dx dy \quad (14)$$

which enables coupling length of only few microns in the case of TM0 to TM3 coupling using the sinusoidal grating presented in section 3.

The proposed device is actually a co-directional coupler which couples two eigenmodes propagating along the same direction in a single multimode waveguide. Solving the coupled mode equation [Eq. (11)] in a case of co-directional coupler, would reveal a periodic exchange of power between the modes along the propagation [39]. The solution of the coupled mode equations in a case of phase matching is

$$A_1(z) = \cos(sz) \cdot A_1(0) - i \frac{\kappa_{12}^{(q)}}{s} \sin(sz) \cdot A_2(0) \quad (15)$$

$$A_2(z) = -i \frac{\kappa_{12}^{(q)*}}{s} \sin(sz) \cdot A_1(0) + \cos(sz) \cdot A_2(0) \quad (16)$$

where  $s^2 = \kappa_{12}^{(q)} \kappa_{12}^{(q)*} + \left(\frac{\Delta\beta}{2}\right)^2$  and  $\Delta\beta = \beta_m - \beta_j - \frac{2\pi q}{\delta}$ .